Kp forecast models

S. Wing,[1] J. R. Johnson,[2] J. Jen,[1] C.-I. Meng,[1] D. G. Sibeck,[3] K. Bechtold,[1] J. Freeman,[5] K. Costello,[6] M. Balikhin,[4] and K. Takahashi[1]

Received 25 March 2004; revised 21 December 2004; accepted 27 January 2005; published 9 April 2005.

[1] Magnetically active times, e.g., Kp > 5, are notoriously difficult to predict, precisely the times when such predictions are crucial to the space weather users. Taking advantage of the routinely available solar wind measurements at Langrangian point (L1) and nowcast Kps, Kp forecast models based on neural networks were developed with the focus on improving the forecast for active times. To satisfy different needs and operational constraints, three models were developed: (1) a model that inputs nowcast Kp and solar wind parameters and predicts Kp 1 hour ahead; (2) a model with the same input as model 1 and predicts Kp 4 hour ahead; and (3) a model that inputs only solar wind parameters and predicts Kp 1 hour ahead (the exact prediction lead time depends on the solar wind speed and the location of the solar wind monitor). Extensive evaluations of these models and other major operational Kp forecast models show that while the new models can predict Kps more accurately for all activities, the most dramatic improvements occur for moderate and active times. Information dynamics analysis of Kp suggests that geospace is more dominated by internal dynamics near solar minimum than near solar maximum, when it is more directly driven by external inputs, namely solar wind and interplanetary magnetic field (IMF).

Citation: Wing, S., J. R. Johnson, J. Jen, C.-I. Meng, D. G. Sibeck, K. Bechtold, J. Freeman, K. Costello, M. Balikhin, and K. Takahashi (2005), Kp forecast models, *J. Geophys. Res.*, *110*, A04203, doi:10.1029/2004JA010500.

1. Introduction

[2] As technology advances, space weather prediction has become increasingly important to our nation's defense, commerce, and research activities. For example, space weather can affect communications, navigation systems, satellite health, power grids, and space travel. Kp is one of the most common indices used to indicate the severity of the global magnetic disturbances in near-Earth space. Kp is an index based on the average of weighted K indices at 13 ground magnetic field observatories. It is based on the range of the magnetic field variation within 3 hour intervals that is caused by phenomena other than the diurnal variation and the long-term components of the storm time variations. The values of the Kp range from 0 (very quiet) to 9 (very disturbed) in 28 discrete steps, resulting in values of 0, 0+, 1−, 1, 1+, 2−, 2, 2+, ...9. The Kp index was first introduced by *Bartels* [1949] and has been published by the Institut für Geophysik der Universität Göttingen since 1949. It was extended backward to 1932 in 1951. Thus the name Kp has a German origin and is an acronym for "planetarische Kennziffer," which simply means planetary index. One Kp value is produced for each 3 hour interval of universal time (UT) at 0–3, 3–6, 6–9, ...21–24. The previous month or older Kp values and other Kp related information are available at GeoForschungsZentrum (GFZ), Postdam, Germany Web site (http://www.gfz-potsdam.de/pb2/pb23/GeoMag/niemegk/kp_index/) and several of its mirror sites, including at the USA's National Oceanographic and Atmospheric Administration (NOAA) (ftp://ftp.ngdc.noaa.gov/STP/GEOMAGNETIC_DATA/INDICES/KP_AP/). A review of the Kp derivation method was given by *Rostoker* [1972].

[3] The relatively long, uninterrupted Kp record since 1932 makes this index useful for studying solar wind-magnetosphere interactions and space weather. There have been many studies that show the correlations between Kp and various parameters of the solar wind and interplanetary magnetic field (IMF) [e.g., *Papitashvili et al.*, 2000; *Crooker and Gringauz*, 1993; *Garrett et al.*, 1974]. Kp has also been shown to correlate to many geospace phenomena. For example, the location of the substorm injection has been shown to have a Kp dependence [*Mauk and McIlwain*, 1974]. The stretching of the field line, the earthward boundary of the plasma sheet, and the ion isotropy boundary have been shown to correlate well with Kp [*Wing and Newell*, 2003; *Newell et al.*, 1998; *Sergeev et al.*, 1993]. Kp also plays significant roles in space weather, e.g., many satellite operators use Kp to estimate satellite drag. Many magnetospheric and ionospheric models require

[1]Johns Hopkins University Applied Physics Laboratory, Laurel, Maryland, USA.
[2]Princeton Plasma Physics Laboratory, Princeton University, Princeton, New Jersey, USA.
[3]NASA Goddard Space Flight Center, Greenbelt, Maryland, USA.
[4]Department of Automatic Control and System Engineering, University of Sheffield, Sheffield, UK.
[5]Physics and Astronomy Department, Rice University, Houston, Texas, USA.
[6]NASA Lyndon B. Johnson Space Flight Center, Houston, Texas, USA.

0148-0227/05/2004JA010500$09.00

Kp as an input parameter. For example, the *Tsyganenko* [1989] magnetic field model, atmospheric density models [e.g., *Hedin*, 1987], ring current–radiation belt models [e.g., *Fok et al.*, 2001], conductivity models [e.g., *Hardy et al.*, 1987], and the Magnetospheric Specification Forecast Models (MSFM) (J. W. Freeman, The magnetospheric specification and forecast model, unpublished manuscript, 1995, available at http://hydra.rice.edu/freeman/ding/www/msfm95/index.html) all require Kp as an input parameter. Also, the recently developed Oval Variation, Assessment, Tracking, Intensity, and Online Nowcasting (OVATION) model can use Kp as an input parameter to determine the equatorial boundary of the auroral oval [*Newell et al.*, 2002]. For space weather, what the models such as MSFM and OVATION do, in effect, is to take Kp, which provides qualitative alerts and use it to produce more quantitative alerts, such as magnetospheric/ionospheric particle fluxes and electromagnetic fields, auroral oval location and fluxes, etc. As a result, precautionary measures could be taken to avoid or reduce catastrophic damage to power grids and satellites.

[4] As a global geomagnetic activity index, Kp has some flaws, although other indices have their own difficulties. The midlatitude locations (48°–63° magnetic latitude) of the 13 midlatitude stations used to compute Kp render it rather difficult for deducing the source(s) of its variations, leading to some ambiguities in its interpretations. Therefore as space physics advances, Kp will probably be supplanted by a newer index or parameter that can indicate less ambiguously the state of the magnetosphere. However, for the reasons mentioned in the previous paragraph and continuity of the space weather operations, for now and in the near future, Kp is likely to continue to play some roles in space physics and space weather.

[5] As mentioned, the official Kp is published with a few weeks' delay, which is usually more than adequate for space physics research that analyzes old observations. Unfortunately, this long delay makes it less useful for the space weather operations. For that reason, *Gehred et al.* [1995] developed a nowcast Kp algorithm, which takes real-time data from several magnetometer stations, not necessarily the same ones used for official Kp, and applies a similar method employed by official Kp to derive Kp estimates. The resulting Kp estimates do not always exactly match the official Kps, but the advantage of this algorithm is that it can produce estimated Kps in near real-time. This nowcast Kp has been routinely produced by the United States Air Force (USAF) 55th Space Weather Squadron and made publicly available by NOAA through its Web site.

[6] More recently, *Takahashi et al.* [2001] developed a more sophisticated Kp nowcast algorithm that calculates Kp fairly accurately. The Kp estimates from this model will soon be made publicly available at the Johns Hopkins University Applied Physics Laboratory (JHU/APL) Web site (http://sd-www.jhuapl.edu/UPOS/spaceweather.html).

[7] For the past few years, the Advanced Composition Explorer (ACE) spacecraft, located upstream at Lagrangian point (L1), has been reliably providing solar wind measurements up to ~30–60 min in advance of their arrival at the near-Earth space environment. Therefore Kp forecast models based on solar wind input could use ACE observations to make short-term forecasts. In fact, *Costello* [1997] developed such a model based on an artificial neural network (NN) algorithm. This model is now routinely operational, and its predictions can be obtained at the NOAA Web site (http://www.sec.noaa.gov/rpc/costello/index.html). More recently, *Boberg et al.* [2000] developed their own NN Kp model that also inputs solar wind.

[8] Moderate and high magnetic activities are notoriously difficult to predict [*Joselyn*, 1995], precisely when predictions become more crucial for space weather users. The previous Kp models also exhibit this typical behavior [e.g., *Detman and Joselyn*, 1999]. These models, which were developed at the time when nowcast Kp models were not yet operational, are driven solely by solar wind/IMF. However, it can be reasonably expected that if the model also inputs parameters that give the present and/or the history of the state of the magnetosphere in addition to the solar wind/IMF driver, the predictions would improve. For example, *Johnson and Wing* [2004, 2005] show that past Kps have strong linear and nonlinear correlations with future Kps.

[9] This paper presents new Kp models that have significantly higher forecast accuracies than the previous Kp operational models. In order to satisfy different needs and operational constraints, three different models were developed: (1) a model that inputs nowcast Kp and solar wind parameters and predicts Kp 1 hour ahead; (2) a model with the same input as model 1 and predicts Kp 4 hours ahead; and (3) a model that inputs only solar wind parameters and predicts Kp 1 hour ahead. The 1 hour and 4 hour prediction lead times are just rough estimates for solar wind monitor at L1. Of course, the actual prediction lead times may vary, depending on the solar wind **V** and the location of the solar wind monitor.

2. Data Set

[10] One shortcoming of many early models is that they were trained on a limited data set. For example, the Costello NN was trained on 7 years of data from 1970, 1976, 1978, 1980, 1981, 1982, and 1989, but the limited availability of the solar wind data from IMP-8 effectively reduces the usable Kp data by more than 50% [e.g., see *Wing et al.*, 1995]. The amount of historical solar wind data has multiplied in the time since the Costello model was developed. Because there are dynamical variations over the course of the solar cycle, it is necessary to build a database that can capture such variations to the extent possible. Therefore we built a solar wind and Kp database that spans more than two solar cycles, 1975–2001.

[11] We used the solar wind and IMF data from IMP-8 (1975–1999), Wind (1994–2000), and ACE (2000–2001). The data are publicly available from NASA CDAWeb (http://cdaweb.gsfc.nasa.gov/). The IMP-8 plasma data are publicly available at the MIT IMP-8 Web site (ftp://space. mit.edu/pub/plasma/imp/www/imp.html).

[12] The historical official Kp index is publicly available at GFZ Postdam Web site (ftp://ftp.gfz-postdam.de/pub/home/obs/kp-ap/). Although the historical Kp database is virtually continuous and uninterrupted from 1975 to 2001, the solar wind and IMF data have gaps, effectively reducing the number of Kp data points that can be used for model development.

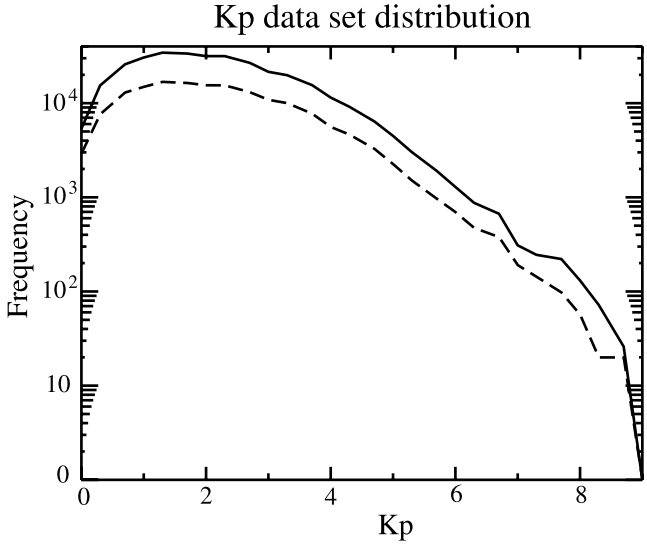

Figure 1. Fifteen-minute interpolated Kp distribution in the data set that spans over two solar cycles, 1975–2001. The test data set (dashed line) has distribution similar to the original full data set (solid line). The y-axis denotes the number of events.

[13] The monthly average International Sunspot Number is available at a NASA Web site (http://science.nasa.gov/ssl/pad/solar/sunspots.htm).

3. Method

[14] This study used an NN paradigm to construct the Kp models. An NN is a mathematical model that attempts to mimic the computation performed by the neurons in the human brain. The advantage of this computational paradigm is that it can be easily adapted to solve a wide range of problems that involve linear and/or nonlinear mappings between a set of input to a set of output. NNs have been increasingly used to solve many problems in space physics, particularly as predictors of time series data. In addition to the two NN Kp prediction models mentioned above, NNs have been used to predict relativistic electron flux at geosynchronous orbit [*Koons and Gorney*, 1991], energetic storm particle (ESP) events impinging on the Earth [*Vandegriff et al.*, 2005], geomagnetic storm [*Wu and Lundstedt*, 1997], etc. NNs have also shown great promises as signal/data classifiers. For example, an NN was used to classify geospace physical boundaries in the plasma data [*Newell et al.*, 1990, 1991]. More recently, an NN was used to classify high-frequency (HF) radar backscattered signals [*Wing et al.*, 2003].

[15] In this study we experimented with two types of general NN architectures: (1) the standard multilayered feedforward–backpropagation network [*Rumelhart and McClelland*, 1987] and (2) the recurrent network in which the outputs of the hidden nodes are fed back to inputs [*Gershenfeld*, 1999; *Fernandez et al.*, 1990; *Lo and Bassu*, 1999]. We compared the best models in each architecture and found that there is no significant difference in their performance. However, in general, the recurrent networks can be trained more quickly than the feedforward–backpropagation networks. Therefore our final models use recurrent network architecture. In this study, all the NN models use one hidden layer. The optimal number of hidden nodes was empirically determined by systematically varying the number of hidden nodes between 4 and 20, or higher if needed. It turns out that most models reach the optimal performances when the number of hidden nodes ranges from 8 to 12. The NN only has one output node, which is Kp. In addition, we developed a simple linear empirical function that maps the NN output to observed Kp. The function has the form of observed Kp = ($a \times$ NN Kp) + b, where a and b are derived empirically from training data sets. We note that this linear correction would only work if NN Kp is already very good. It would not work (e.g., the scatter would be too large) if the model output Kp was terrible to begin with. The final predicted Kp is the output of this function, which acts as a postprocessor for the NN.

[16] For the purpose of training and testing NNs, the solar wind/IMF and Kp data set from 1975–2001 was randomly selected to form two equal subsets: (1) a training set and (2) a test set. To estimate the arrival time of the solar wind and IMF in the Earth space environment, the solar wind/IMF were propagated to Earth (X = 0) with the assumption that the planar solar wind phase front is perpendicular to the Sun-Earth line (ballistic propagation). Then, solar wind density (n), and velocity (**V**) and IMF were hourly averaged at 15 min time intervals, which is the time granularity of the model outputs. In order to match the time granularity of Kp (3 hours) to the model (15 min), the Kps are interpolated to 15 min resolution. This is done by time-tagging the Kp with the center of the 3 hour interval, e.g., at 0130, 0430, 0730 UT, etc., and then linearly interpolating between those points. For operational considerations, 15 min is preferred over the traditional 3 hour time granularity. With 15 min time granularity, the models can warn the users of the impending change in the space weather more quickly. For example, using 15 min time granularity, if a satellite at L1, e.g., ACE, detected a sudden change in the solar wind that would cause a huge increase in geomagnetic activity, the model would be able to warn the users with a new and higher Kp in the next 15 min, before the actual arrival of the solar wind. On the other hand, using the traditional Kp 3 hour time resolution, the model would not be able to broadcast the impending catastrophic condition for up to the next 3 hours, which might be too late for many operations. For practical purpose, the model 15 min Kp value can be treated as the traditional 3 hour Kp value, as is presently done in Costello model.

[17] In Figure 1, the solid line shows the distribution of the interpolated 15 min resolution Kp data points that have corresponding good simultaneous solar wind and IMF observations. In other words, the solid line essentially shows the total number of data points that can be used for our study. The dashed line shows the Kp data in the test set. Figure 1 basically shows that the test data set has roughly the same distribution as the original full data set and hence has no bias.

4. Previous Kp Models

[18] For the purpose of model comparisons, three existing operational Kp prediction models are considered: (1) Cost-

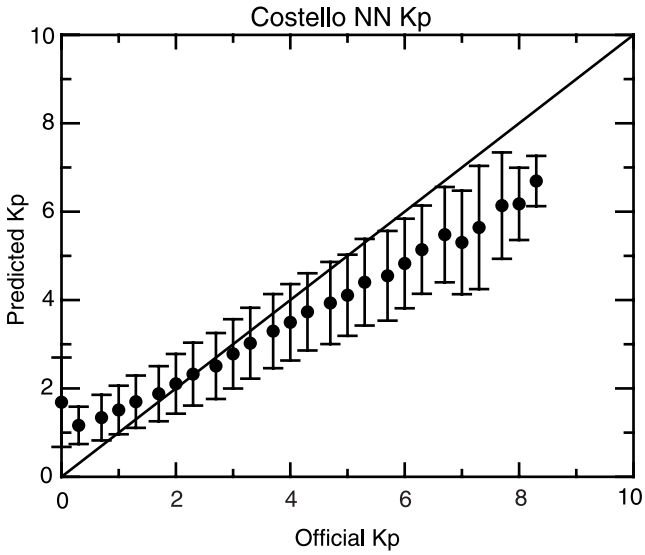

Figure 2. The performance of the Costello NN model, which predicts Kp 1 hour ahead. NOAA routinely provides this model's predictions. Official (Postdam) Kp is plotted on the x-axis and the model prediction is plotted on the y-axis. Perfect predictions would lie on the line with a slope of one. The error bar indicates one standard deviation.

ello NN, (2) NARMAX, (3) Boberg et al. NN. All these models predict Kp roughly 1 hour ahead using a solar wind monitor located at L1. In order to subject the models to the same evaluation procedure and test data set, the Costello NN and NARMAX models were ported to our computer. We have no access to the Boberg et al. model and hence the comparison with this model is more limited.

4.1. Costello NN Kp Model

[19] Presently, NOAA routinely provides real-time short-term Kp forecasts from the most popular Kp prediction model, the Costello NN Kp model [*Costello*, 1997] (http://www.sec.noaa.gov/rpc/costello/index.html). This model inputs ACE solar wind speed and IMF Bz and $|\mathbf{B}|$ and predicts Kp roughly 1 hour ahead every 15 min. The actual prediction lead time may vary, depending on the solar wind **V**. In order to facilitate careful and systematic comparisons with other models, this model was ported to our computer at JHU/APL. Figure 2 shows the results of running the model on the test data set shown in Figure 1. Figure 2 shows that the model predictions are fairly accurate during quiet times (Kp < 5) but are less accurate during moderate or active times (Kp > 5), a typical problem for many models [*Joselyn*, 1995] and a feature that likely results from the low number of high Kp events captured in the training data set [*Costello*, 1997]. This behavior is also consistent with the previous evaluation of Costello model [*Detman and Joselyn*, 1999]. The correlation coefficient (r) between the forecast and official Kp is 0.75.

4.2. NARMAX Kp Model

[20] We also ported a NARMAX Kp model that was developed at the University of Sheffield, UK. NARMAX is an acronym of Nonlinear Auto Regressive Moving Average Models With Exogenous Inputs and is described by *Balikhin et al.* [2001] and *Boaghe et al.* [2001]. The model inputs solar wind speed and dynamic pressure, IMF $|\mathbf{B}|$, Bz, and optionally a previous Kp (Kp at time = t − 3 hours, where t is the solar wind arrival time on Earth). The previous Kp could be its own previous prediction (feedback mode) or a Kp estimate, i.e., a nowcast Kp. Over time, the model performs more poorly if it inputs its own prediction rather than nowcast Kp. Figure 3 shows the NARMAX Kp performance using the same test data set and a nowcast Kp (see section 5.1 for more discussion on nowcast Kp) as an input parameter. From Figures 2 and 3, it can be seen that NARMAX model predicts high Kps slightly better than the Costello NN model, although the predictions of the former have larger scatter. The correlation coefficient r = 0.77, which is comparable to or just slightly higher than that of the Costello model.

4.3. Boberg et al. NN Kp Model

[21] *Boberg et al.* [2000] developed a Kp forecast model that is also based on an NN. Because we do not have access to this model, we cannot evaluate this model using the same procedure and test data set used for the other models evaluated in this study. Instead, we rely on their own evaluation of their model as presented in the work of *Boberg et al.* [2000]. Fortunately, they also present a predicted Kp versus official Kp plot (see Figure 4 in the work of *Boberg et al.* [2000]), which can be compared with similar plots in this paper, for example, Figures 2 and 3 with the above-mentioned caveat. They report correlation coefficient r = 0.77, which is roughly comparable to those obtained by the NARMAX and Costello models. Like these two models, their result indicates that their model does not predict active times as well as quiet times. Their model inputs solar wind **V**, n, and IMF Bz.

5. APL Kp Models

[22] We developed three different Kp models: (1) a model that inputs nowcast Kp and solar wind parameters and predicts Kp 1 hour ahead; (2) a model with the same input

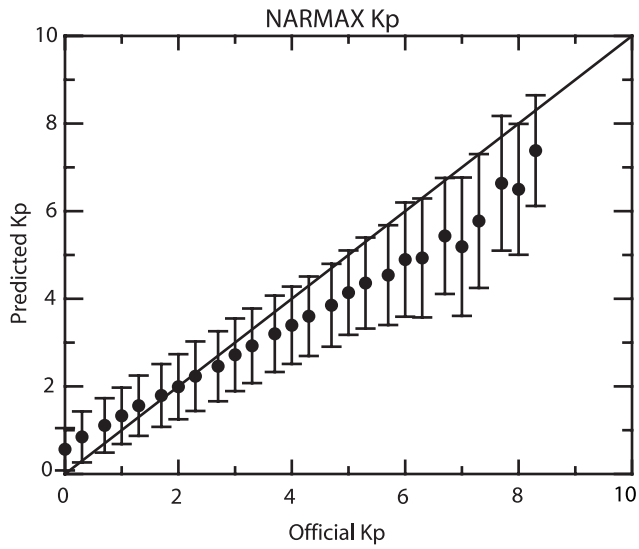

Figure 3. NARMAX 1 hour ahead Kp performance shown in the same format as Figure 2.

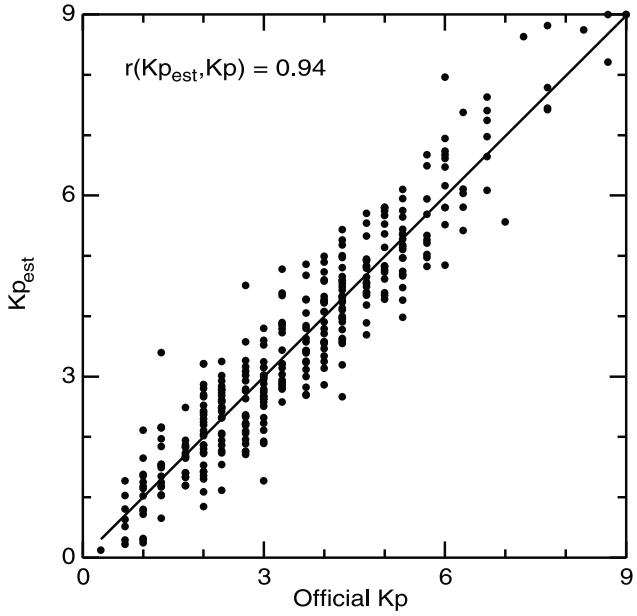

Figure 4. Performance of *Takahashi et al.* [2001] nowcast Kp estimate algorithm for days 70–120 in 1989, a 50-day period that includes an extremely strong magnetic storm. The x-axis displays the official (Postdam) Kp. The magnetometer data for Kp estimates come from only three stations: Fredericksburg, Newport, and Sitka (from Figure 13 of *Takahashi et al.* [2001]).

as model 1 and predicts Kp 4 hours ahead; and (3) a model that inputs only solar wind parameters and predicts Kp 1 hour ahead.

5.1. Kp Model That Inputs Solar Wind and Nowcast Kp and Predicts Kp 1 Hour Ahead (APL Model 1)

[23] We developed a model (hereinafter referred to as APL model 1) that inputs solar wind |Vx|, n, IMF |**B**|, Bz, and nowcast Kp. Using solar wind measurements at L1, APL model 1 predicts Kp up to approximately 1 hour ahead (the actual prediction lead time may vary, depending on the solar wind **V**). The nowcast Kp algorithm [e.g., *Takahashi et al.*, 2001] at time t can estimate Kp for (t − 1.5 hours). For simplicity in building the model, the model inputs a Kp estimate for time (t − 1.25 − 1.5 hours) or (t − 2.75 hours), where t is the solar wind/IMF arrival time on Earth. This assumes that most of the times the solar wind monitor at L1 would provide solar wind measurements <1.25 hours in advance. Since the nowcast Kp algorithm has only recently become available, for model development, the input Kp comes from the official Kp record that spans over two solar cycles. However, for model evaluation, the input Kp comes from two sources: (1) the official Kp record and (2) the Kp estimates from *Takahashi et al.* [2001] algorithm. Of course, the official Kps are used to determine the accuracy of the forecast Kps. The advantage of source 1 is that it covers a large time interval, 1975–2001, but the disadvantage is that the evaluation gives only a sense of the upper bound performance. The advantage of source 2 is that it gives a realistic evaluation for real-time operations, but since the nowcast Kp algorithm was only recently developed, it has a much more limited time coverage. However, the nowcast Kp estimates have improved significantly, having correlation coefficient between nowcast and official Kps of r > 0.9 [*Takahashi et al.*, 2001]. Therefore it is expected that the difference between sources 1 and 2 would be small. Figure 4 presents an example of the performance of *Takahashi et al.* [2001] Kp estimates for days 70–120 in 1989 (from Figure 13 of *Takahashi et al.* [2001]). The Kp estimates were calculated from only three magnetometer stations: Fredericksburg, Newport, and Sitka. The accuracy would improve with additional magnetometers. The *Takahashi et al.* [2001] algorithm can produce a nowcast Kp every 3 hours or at higher time resolution, e.g., every 15 min.

[24] In order to show how well the model works, Figure 5g shows the model prediction over a randomly selected 30 day interval in the test data set. Figures 5a–5f display the time shifted solar wind and IMF during this 30 day interval.

[25] The statistical model evaluation on the test data set (from the official Kp record), as displayed in Figure 6a, shows that model 1 is a significant improvement over previous models. This can be seen by comparing Figure 6a with Figures 2 and 3 of the present paper and with Figure 4 of *Boberg et al.* [2000]. Figure 6a shows that the model predicts Kp well not only during quiet times but also during active times. The correlation coefficient r = 0.92 is far higher than those from the other models.

[26] Model 1 has also been evaluated using *Takahashi et al.* [2001] nowcast Kp as an input parameter, instead of the historical official Kp. For this evaluation, we processed magnetometer data from three stations (Fredericksburg, Newport, and Sitka) for the year 1998 to produce Kp estimates at 15 min resolution. Figure 6b shows the results of the evaluation with these Kp estimates, which are very similar to Figure 6a. The scatter in Figure 6b is perhaps slightly larger for high Kps, which may be attributed partly to fewer data points and partly to inaccuracies in the nowcast Kps. Overall, Figures 6a and 6b suggest that running the model in real-time with *Takahashi et al.* [2001] nowcast Kp as an input parameter would result in performance that does not differ appreciably from that obtained with 15 min interpolated official Kp.

[27] The superior performance of APL model 1 over the previous models could perhaps be attributed to several factors (the square brackets indicate the particular model(s) that lack the corresponding attribute): (1) the model was trained with much larger data set spanning over two solar cycles [Costello, NARMAX]; (2) the model inputs not only solar wind **V**, but also n (hence dynamic pressure) [Costello]; and (3) the model inputs nowcast Kp, which is highly correlated with near-future Kp (see section 6) [Costello, Boberg et al.].

[28] For operational consideration, the *Takahashi et al.* [2001] model will soon be operational at JHU/APL and its nowcast Kps will be made publicly accessible through the Web site given above. Alternatively, APL model 1 can use the nowcast Kps provided at the NOAA Web site given above. The real-time ACE measurements are already routinely publicly accessible at the same NOAA Web site.

5.2. Kp Model That Inputs Solar Wind and Nowcast Kp and Predicts Kp 4 Hours Ahead (APL Model 2)

[29] The second model (hereinafter referred to as APL model 2) inputs the same parameters as APL model 1 but

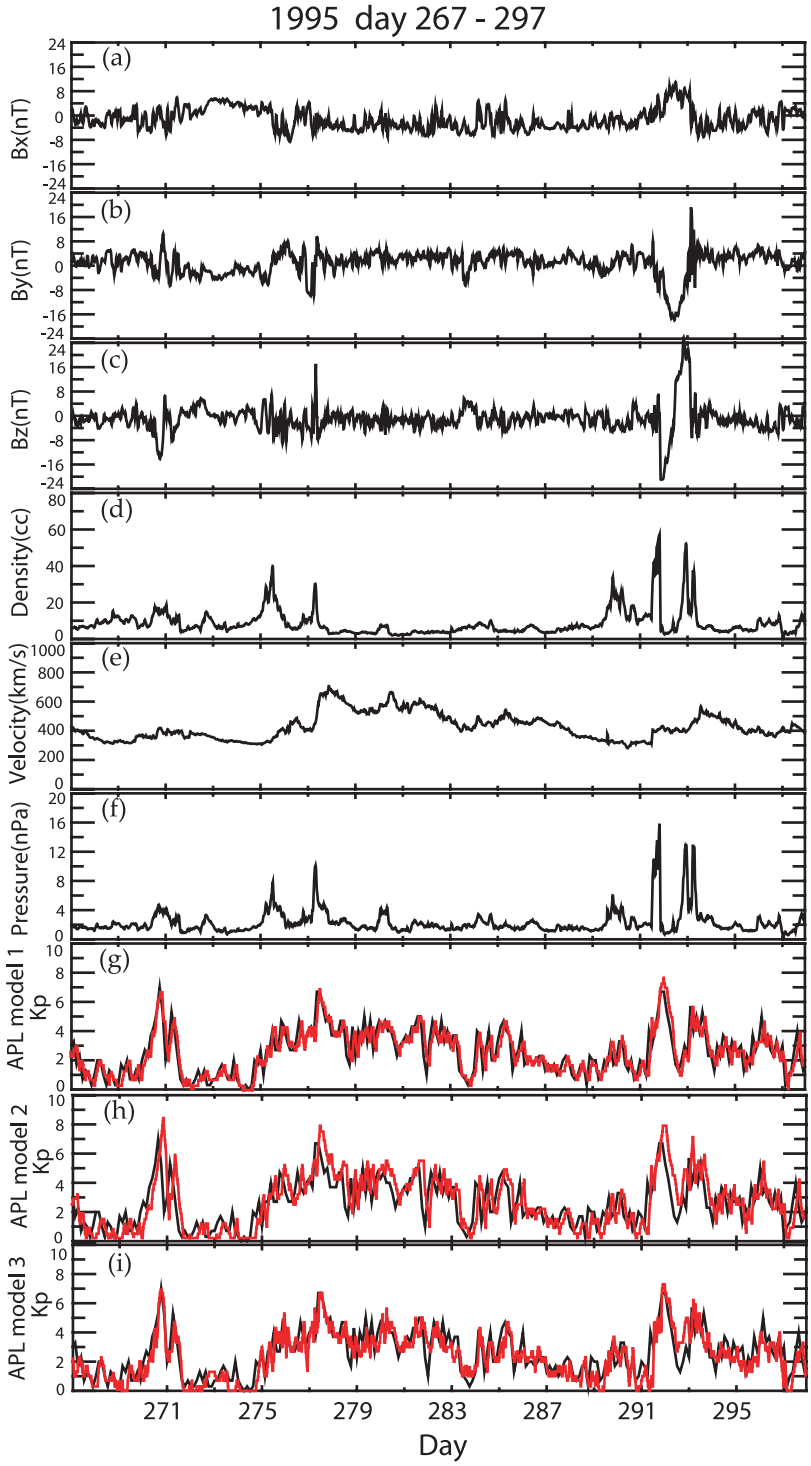

Figure 5. Example of the APL models Kp forecasts on a randomly selected 30 day period in the test data set. (a)–(f) IMF Bx, By, Bz, solar wind density, velocity, and dynamic pressure, respectively. (g)–(i) official Kp (black) and forecast Kp (red [or gray in the black and white version]) for APL models 1, 2, and 3, respectively. The solar wind and IMF have been hourly averaged and time shifted.

predicts Kp 4 hours ahead based on solar wind measurements at L1. Thus unlike APL model 1, this model predicts Kp without knowing the entire history of the solar wind parameter leading up to the forecast time. Specifically, a satellite at L1 provides solar wind parameters only approximately 1 hour ahead, but the model predicts Kp 4 hours ahead. Figure 5h shows the model Kp forecasts over a 30-day interval, which was randomly selected. Figure 7a presents the statistical model performance on the test data set (with input Kp obtained from the official Kp record).

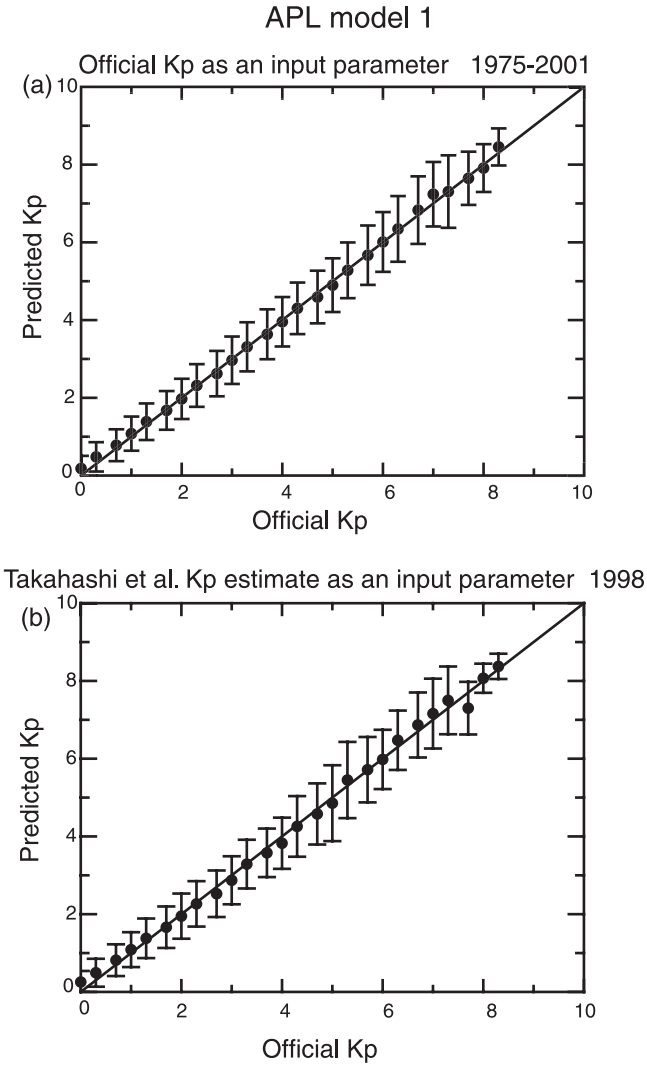

Figure 6. APL NN 1 hour ahead Kp (APL model 1) performance shown in the same format as in Figure 2. This model inputs nowcast Kp from (a) the test data set from the official Kp record 1975–2001 and (b) the *Takahashi et al.* [2001] Kp estimates for 1998. The model is significantly better than Costello NN (Figure 2) and NARMAX (Figure 3).

Figure 7b shows the evaluation using the *Takahashi et al.* [2001] Kp estimate as an input parameter for the year 1998. As expected, the longer prediction lead time results in the reduction in performance. The reduction in performance is manifested in the form of larger scatter compared with that of APL model 1. However, as shown in Figure 7, despite forecasting further ahead in time, the 4 hours ahead Kp forecasts for active times (Kp > 5) are more accurate than the 1 hour ahead forecasts from the Costello, Boberg et al., and NARMAX models. The correlation coefficient, r = 0.79, is slightly higher than that of the other 1 hour ahead Kp forecast models (Costello, NARMAX, and Boberg et al.).

[30] Consistent with the APL model 1 evaluation, the APL model 2 evaluation also demonstrates that running the model in real time with the *Takahashi et al.* [2001] nowcast Kp as an input parameter produces results that are almost as good as those obtained using interpolated official Kp (test data set).

5.3. Kp Model That Inputs Only Solar Wind and Predicts Kp 1 Hour Ahead (APL Model 3)

[31] There may be times (locations) when (where) nowcast Kps are simply not available or reliable. For this reason, we developed a model (hereinafter referred to as APL model 3) that is driven solely by solar wind and IMF. This model inputs solar wind n and |Vx| and IMF |**B**| and Bz. Using solar wind measurements at L1, e.g., ACE, APL model 3 outputs 1 hour ahead Kp forecast. Figure 5i shows

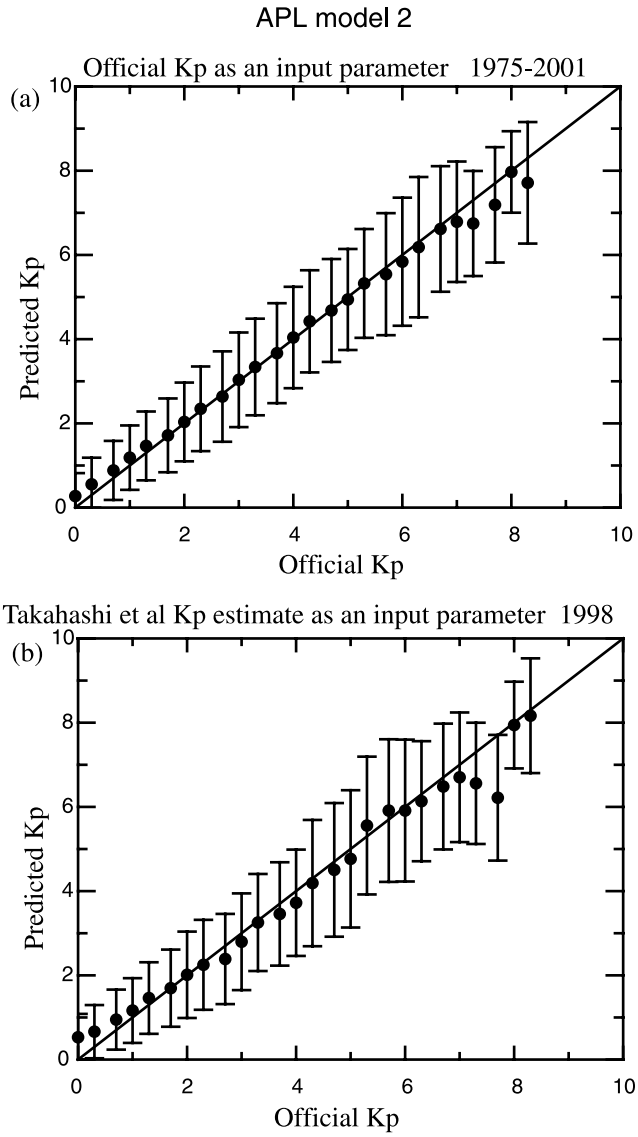

Figure 7. APL Kp NN 4 hours ahead (APL model 2) Kp performance shown in the same format as in Figure 2. (a) The input Kp comes from the test data set (official Kp record), and (b) the input Kp comes from the *Takahashi et al.* [2001] Kp estimate for 1998. Note that the performance for active times, Kp > 5, is better than that of the Costello and NARMAX models, even though its forecast range is 4 hours ahead, whereas those two models predict only 1 hour ahead.

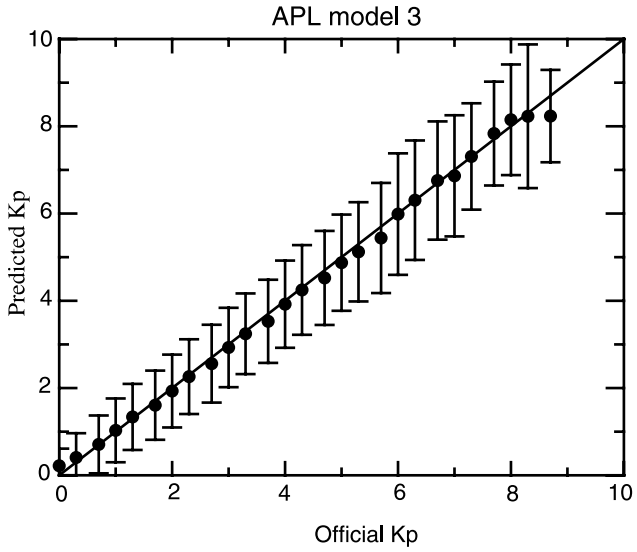

Figure 8. APL Kp NN 1 hour ahead (APL model 3) Kp performance shown in the same format as in Figure 2. This model inputs only solar wind and IMF and no nowcast Kp. This can be directly compared with the Costello NN model results shown in Figure 2, since both models input only solar wind and IMF parameters and no nowcast Kp.

the model outputs over a 30-day period. Figure 8 presents the model performance using the same test data set used throughout this study, except for the Boberg et al. model. It has a correlation coefficient of r = 0.84. Figure 8 shows that without the benefit of the nowcast Kp, the accuracy is lower. Since this model inputs only solar wind and IMF parameters and no nowcast Kp, it can be most directly compared with the Costello and Boberg et al. models, which do not input nowcast Kp either. The comparisons show that despite having the same kind of inputs, APL model 3 still outperforms these two models, albeit the performance improvement is less than for APL model 1. APL model 3 also outperforms the NARMAX model, despite the latter having the advantage of nowcast Kp as an input parameter.

6. Kp (Magnetospheric) Predictability as a Function of Solar Cycle

[32] *Papitashvili et al.* [2000] show that there is a solar cycle variation in the average Kp. The accuracies of nowcast Kps calculated from ground magnetometer data exhibit no discernable correlation with sunspot numbers [*Takahashi et al.*, 2001]. It would be interesting to determine whether the accuracies of the Kp (a proxy for the state of the magnetosphere) forecast based partly or entirely on solar wind/IMF have solar cycle dependence. In order to do this, we calculated the skill scores for the Costello model predictions over two solar cycles, 1975–1999, using IMP-8 solar wind data. NOAA issues alerts when Kp is expected to exceed certain threshold, e.g., 4, 5, 6, etc. Figure 9 plots True Skill Statistics (TSS) and Gilbert Score (GS) for these Kp thresholds [*Detman and Joselyn*, 1999]. In both of these scoring systems, a random prediction = 0 and a perfect prediction = 1. The normalized monthly average International Sunspot Number is plotted at the bottom of Figures 9c–9e. In the present paper, in order to improve the visualization, the sunspot numbers are not normalized to one. Examination of the skill scores and the sunspot numbers in Figures 9c–9e reveals that the Costello model predicts Kp more accurately near solar maximum than minimum.

[33] It is not clear from Figure 9 whether this solar cycle variation is physically significant or whether it results from having a limited training set. Therefore we calculated the same skill scores for different models using a different and larger solar wind data set, namely IMP-8 (1975–1994), Wind (1994–2000), and ACE (2000–2001) solar wind data. An example is shown in Figure 10, which shows the skill scores for APL model 3 in a format similar to Figure 9. This model, which was trained with a much larger data set spanning over two solar cycles, inputs only solar wind/IMF as in Costello model. Training with larger data sets helps improve the accuracy of the predictions and significantly reduces the solar cycle variation, but it does not appear to completely eliminate the solar cycle effect. In Figures 10a–10d, the skill scores appear to exhibit mild solar cycle variations, but the maxima and minima of the sunspot number do not always appear at the same time as those of the skill scores. The maxima of the skill scores often appear during the declining phase of the solar maximum. Figures 9 and 10 would suggest that at least a component of the solar cycle variation might result from a more fundamental way in which solar wind interacts with the geospace.

[34] Recently, we applied a cumulant-based method to analyze the statistical informational dynamics of Kp time series and found that there is a stronger nonlinear relationship between past Kp and future Kp around solar minimum than around maximum [*Johnson and Wing*, 2004, 2005]. This relationship is depicted in Figure 11, which plots the normalized linear (SL) and nonlinear (SNL) significance as a function of time delay, τ, in hours for Kp data for two solar minima (Figures 11a and 11c) and two solar maxima (Figures 11b and 11d). For time T, SL is roughly proportional to the linear correlation between Kp(T) and Kp(T $-$ τ), whereas SNL gives a measure of the nonlinear correlations. The details of the calculations are given by *Johnson and Wing* [2004, 2005]. The figure shows that while the linear response is roughly the same around solar minimum and maximum, the nonlinear response is stronger for solar minimum than maximum, with a peak around $\tau \sim 40$ hours.

[35] It turns out that the nonlinear response (SNL) anticorrelates with sunspot number in every solar cycle since the Kp index has been recorded, 1932 to the present (2003). Figure 12 shows clearly this anticorrelation in two different ways: Figure 12a shows the maximum SNL, and Figures 12b–12c show the integrated SNL for >95% and >99.5% confidence, respectively, for years 1932–2003. Figure 12 was obtained from the yearly SNL curves such as the ones shown in Figure 11. For easy reference, the normalized sunspot number is plotted as lighter (gray) lines at the bottom of each panel. In Figure 12a, the probability that a linear model could produce significance of 10 is $1{:}10^{23}$. The integrated significance sums over all correlation times up to $\tau = 200$ hours and may give a better indicator of the presence of nonlinearity over long times than just the maximum value. It is only appropriate to compare the relative value of the integrated significance within each plot. The typical

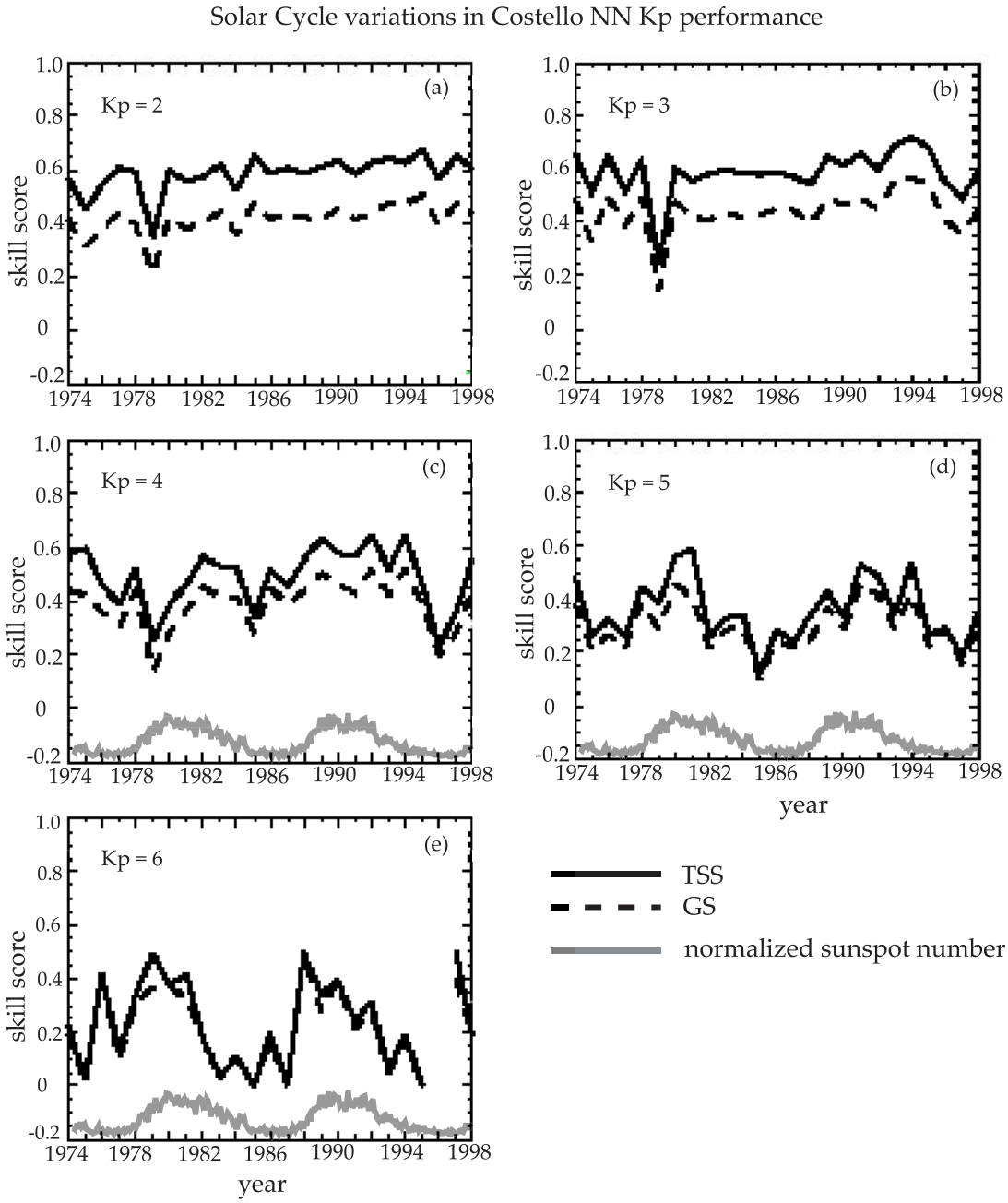

Figure 9. The Costello model predicts Kp more accurately near solar maximum than near solar minimum for Kp > 3. (a)–(e) Skill scores for the Costello NN Kp model over two solar cycles for Kp = 2–6, respectively. The black solid line = True Skill Statistic (TSS) and the dashed line = Gilbert score (GS). The lighter (gray) solid lines at the bottom of Figures 9c–9e indicate the normalized monthly average International Sunspot Number, which exhibits trends similar to the skill scores.

correlation time for high nonlinear significance events lies around 40 hours (see also *Johnson and Wing* [2004, 2005]). The timescale over which the nonlinear significance is appreciable is on the order of a week. These timescales are similar to timescales associated with ring current relaxation (hours to days) and storm relaxation (1 week).

[36] Taken together, these nonlinearities and the skill scores suggest that around solar minimum, the magnetosphere is dominated more by internal dynamics than it is around solar maximum, when it is more directly driven by the external inputs, namely solar wind and IMF. The presence of the internal dynamics would complicate the Kp predictions that rely entirely or partly on the external drivers.

[37] The statistical information dynamical analysis of Kp shown in Figure 11 indicates that Kp highly correlates with

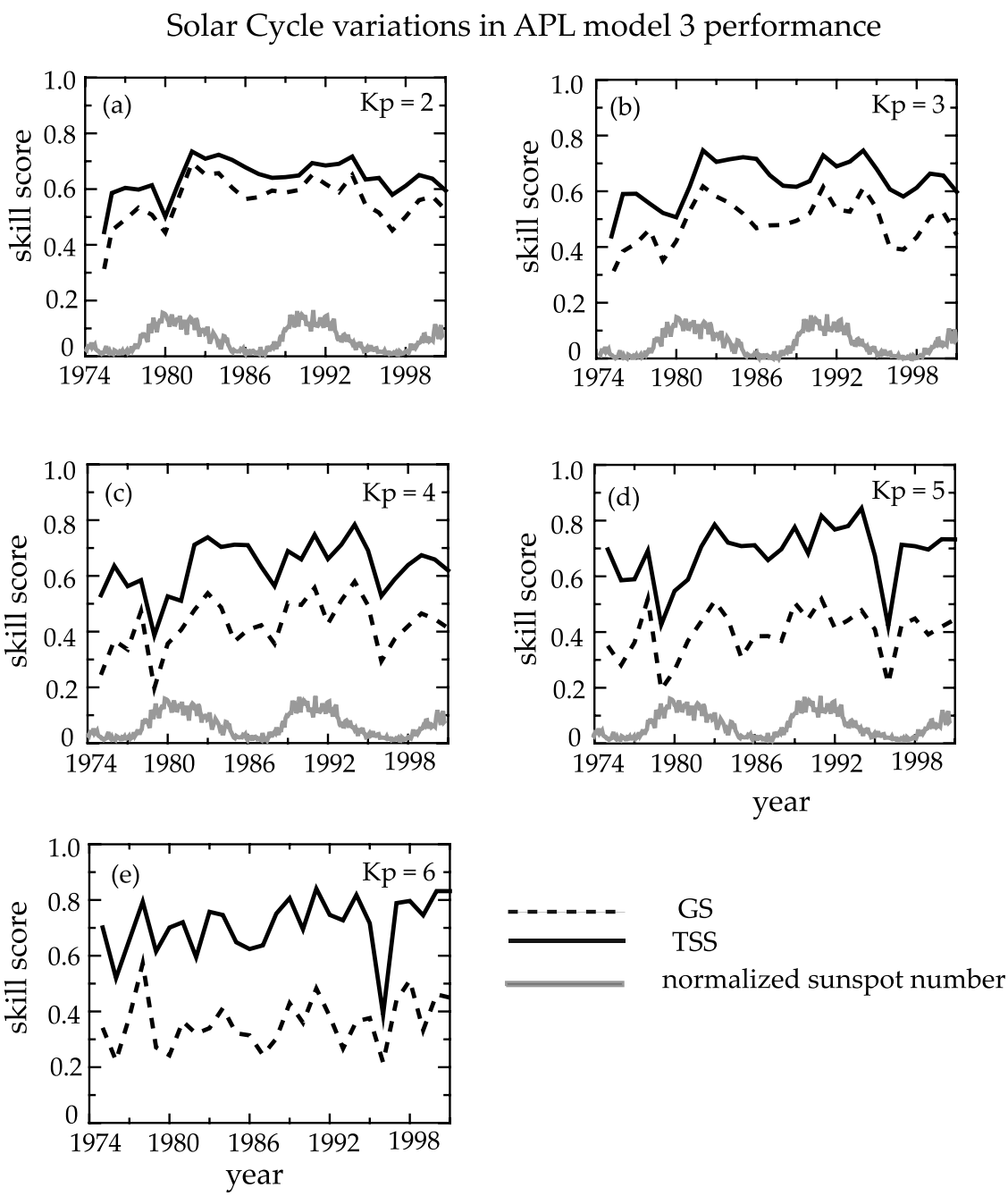

Figure 10. Skill scores over two solar cycles for a Kp model that inputs solar wind parameters and predicts Kp 1 hour ahead (APL model 3). (a)–(e) Skill scores for APL model 3 for Kp = 2–6, respectively. The black solid line = True Skill Statistic (TSS) and the dashed line = Gilbert score (GS). The lighter (gray) solid lines at the bottom of Figures 10a–10d plot the normalized monthly average International Sunspot Number. In Figures 10a–10d, while the skill scores are higher than those for the Costello model, they still exhibit yearly variations that roughly follow the same general pattern as the sunspot number.

the past Kps within the last few hours, linearly and nonlinearly (the Kp has been interpolated to 15 min resolution). Therefore including the nowcast Kp can improve the 1 hour ahead Kp forecasting. However, both the linear and nonlinear correlations drop off sharply with increasing τ, which contribute to the rapid decrease in the performances of APL model 2 compared with APL model 1.

[38] Near solar minimum, as shown in Figure 11, there are significant nonlinear correlations between Kp and past Kps that may be attributed to internal dynamics. Thus in theory the nowcast and all past Kps may help improve the Kp forecasts, since they contain some information that pertains to the internal dynamics, including persistence. This information is not available in the solar wind/IMF.

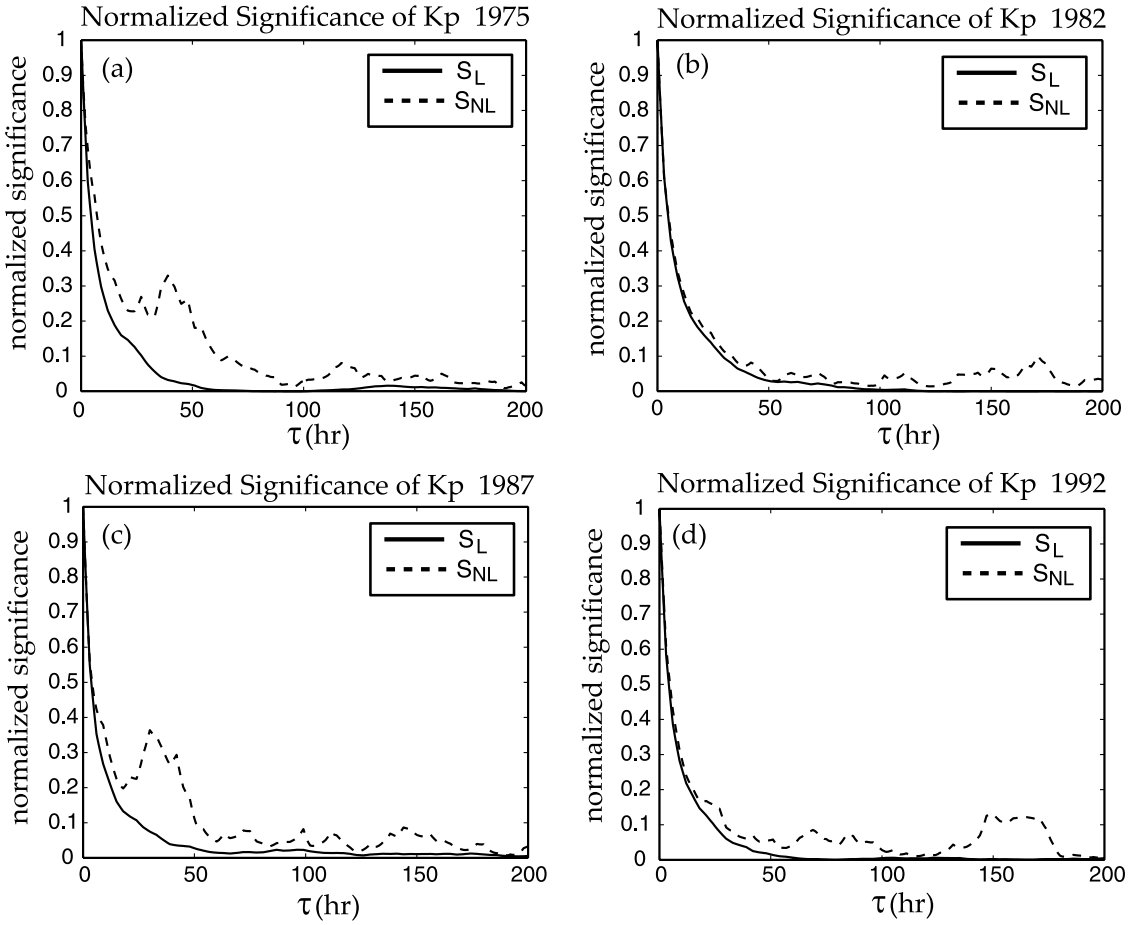

Figure 11. Normalized linear (SL) and nonlinear (SNL) significance as a function of time delay τ, for Kp data from near (a) solar minimum 1975, (b) solar maximum 1982, (c) solar minimum 1987, and (d) solar maximum 1992. SL is proportional to the linear correlation coefficient between Kp(T) and Kp(T $-$ τ), whereas SNL gives a measure of the nonlinear correlation. SL = solid line and SNL = dashed line. SL drops off quickly with increasing τ for both solar maxima and minima. Near solar minima, there is a strong nonlinear response with a peak around τ = 40 hours, whereas near solar maxima, SNL tapers off quickly.

The recurrent NN has some capacity to memorize the past Kps (for APL models 1 and 2), but it is doubtful that it can effectively capture the complex correlations or dynamics beyond the last few hours (the nonlinear correlations can extend beyond several hours).

7. Discussion and Summary

[39] In order to satisfy different needs and operational constraints, we developed three types of Kp forecast models, two of which require nowcast Kp as an input parameter. The focus of the model development was improving the forecasts for magnetically moderate and disturbed times, which are notoriously difficult to predict [e.g., *Joselyn*, 1995]. The three models are (1) APL model 1 that inputs nowcast Kp and solar wind parameters and predicts Kp 1 hour ahead; (2) APL model 2 that has the same input as APL model 1 and predicts Kp 4 hours ahead; and (3) APL model 3 that inputs only solar wind parameters and predicts Kp 1 hour ahead. The 1 and 4 hour prediction lead times are just rough estimates for a solar wind monitor at L1. The actual prediction lead times may vary, depending on the solar wind **V** and the location of the solar wind monitor. All these models are based on NNs and were developed with 27 years of data, 1975–2001.

[40] Our extensive evaluation based on data spanning more than two solar cycles shows that (1) our models give significantly more accurate predictions than previous models, with the most dramatic improvements occurring during moderate and active times, Kp > 4, and (2) Kp is slightly more predictable near solar maximum than it is near solar minimum. Information dynamics analysis of Kp suggests that the magnetosphere is more externally driven near solar maximum (or the declining phase of the solar maximum) than near solar minimum. Around solar minimum, the internal dynamics such as loading and unloading of the energy in the magnetotail, ring current decays, storm relaxation, etc., may play a more important role in the magnetospheric dynamics and may introduce some difficulties to Kp models that rely entirely or partly on solar wind parameters.

[41] The performances of various models can be summarized in Figure 13, which plots the TSS scores of the Kp threshold [*Detman and Joselyn*, 1999]. Figure 14 summa-

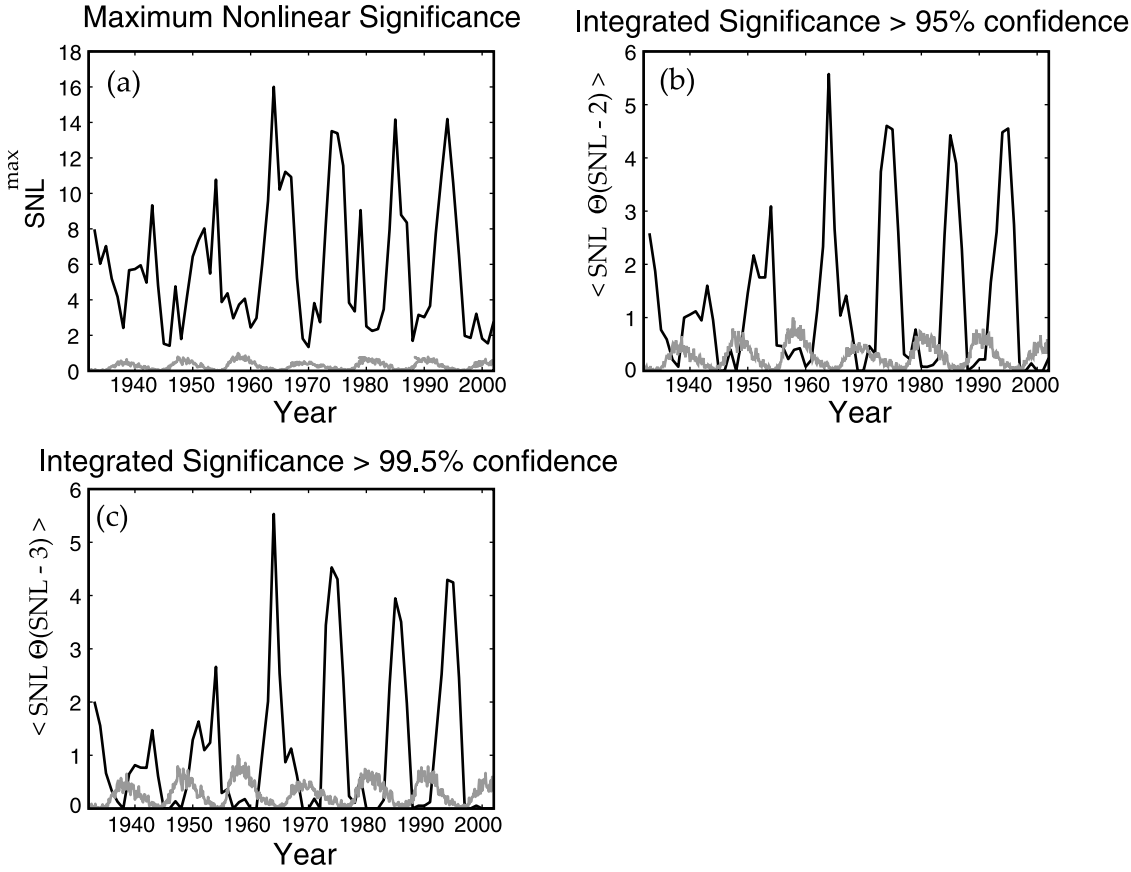

Figure 12. The nonlinear response anticorrelates with the sunspot number in every solar cycle from the first Kp record to present, 1932–2003. (a) The black line shows the maximum nonlinear significance (SNL); (b) and (c) the black line shows the integrated SNL at >95% confidence and at >99.5% confidence, respectively. The lighter (gray) lines at the bottom in Figures 12a–12c show the normalized sunspot number.

rizes the correlation coefficients for all the models, which is fairly consistent with the skill scores. For comparisons with other published model evaluations, the correlation coefficient r is calculated here for all Kp ranges. Therefore Figure 14 understates the dramatic improvements in the active times (Kp > 5) forecast range achieved by APL Kp models. We also note that r, by itself, does not indicate how well the model performs. For example, it would be possible to have a model that systematically and consistently underpredicts Kp but does so with little scatter and high r. Thus comprehensive model evaluations should include scatterplots (e.g., Figures 2, 3, 6, 7, 8), skill scores, and r.

[42] The advantage of having nowcast Kp can be seen, at least qualitatively, by comparing model 1 and model 3, e.g., comparing Figures 6 and 8. The advantage of larger data sets plus inclusion of solar wind density can be seen by comparing APL model 3 with the Costello model, e.g., Figures 2 versus 8. However, the quantifications of these effects would require substantially more work and should be addressed in the future work.

[43] For operational consideration, nowcast Kps, based on an Air Force algorithm, are now routinely made publicly available by NOAA. Furthermore, *Takahashi et al.* [2001] have developed a very accurate nowcast Kp algorithm. These nowcast Kps will soon be publicly available at a

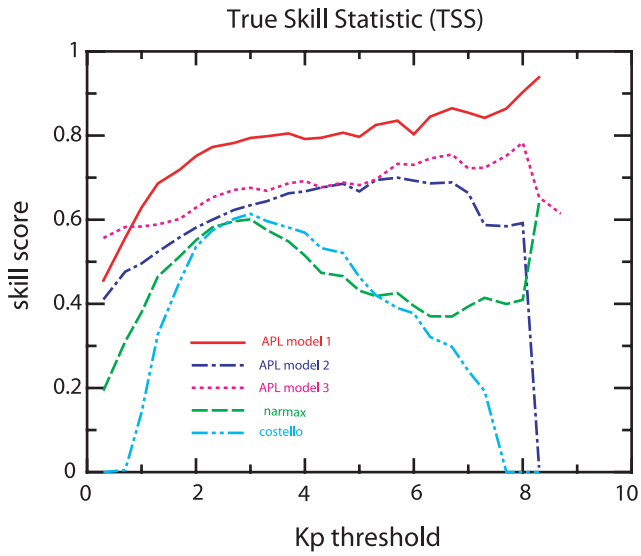

Figure 13. APL Kp models outperform the existing Kp forecast models. True Skill Statistic (TSS) as a function of Kp threshold for APL model 1 (red), APL model 2 (blue), APL model 3 (purple), the NARMAX model (green), the Costello model (cyan).

JHU/APL Web site once the live magnetometer data streams become available. Our study demonstrates that these nowcast Kps can be used to improve the forecast Kps. Thus APL models 1 and 2 can be used whenever nowcasts Kps are available, while APL model 3 can be used when only solar wind/IMF measurements are available.

[44] For practical and operational considerations, the APL models predict a new Kp every 15 min instead of every 3 hours. The higher time resolution was chosen to enable the models to warn users of the impending change in space weather in a more timely manner. For example, using 15 min time granularity, if ACE detected a sudden change in the solar wind that would cause a huge increase in geomagnetic activity, the model would be able to warn the users in the next 15 min, before the actual arrival of the solar wind, whereas using the traditional Kp 3 hour time granularity, the model would not be able to do so. All model evaluations presented so far are done by comparing the model output Kp at 15 min granularity with the 15 min interpolated historical official Kp. This is deemed more accurate than the comparisons with the historical 3 hour Kp because the magnetospheric state changes in a continuous manner rather than in 3 hour step function. However, we have also statistically evaluated the model output Kp against the traditional 3 hour official Kp in a similar manner as in Figures 6–8, 13, and 14. The results do not show appreciable differences with those evaluations against the interpolated 15 min Kp presented above. Figure 15 shows two examples: for APL model 2 (Figure 15a) and for APL model 3 (Figure 15b). Thus for practical purpose, the model output 15 min Kp could be treated as the traditional 3 hour Kp. Evaluated in this manner, APL Kp models still outperform the existing Kp models.

[45] The APL Kp models can provide a short-term forecast, up to a few hours ahead using solar wind/IMF measurements at L1. These short-term forecasts would be valuable for space weather users, but for many applications longer-term forecasts are more desirable. We would like to note that there are several heliospheric models that are currently operational and/or under various stages of development. These models input solar observations and predict solar wind/IMF days in advance, e.g., the Hakamada-Akasofu-Fry (HAF) code [*Fry et al.*, 2001; *Hakamada and Akasofu*, 1982] and the Wang-Sheeley model [*Wang and Sheely*, 1995; *Arge and Pizzo*, 2000]. Also, the NASA Living With a Star (LWS) roadmap calls for the launch of a multispacecraft space weather network (Solar Dynamics Observatory and Sentinels) with a main goal of providing the solar wind parameters with longer lead time (http://lws.gsfc.nasa.gov). Thus the APL Kp model 3, which is driven solely by solar wind/IMF, can be linked with these models/products to provide longer-term forecasts.

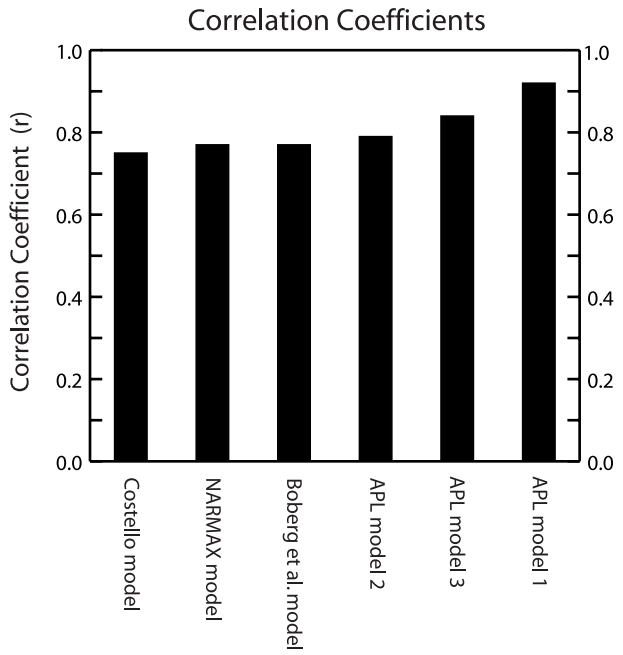

Figure 14. Correlation coefficients for the three APL models, and the Costello, NARMAX, and Boberg et al. models.

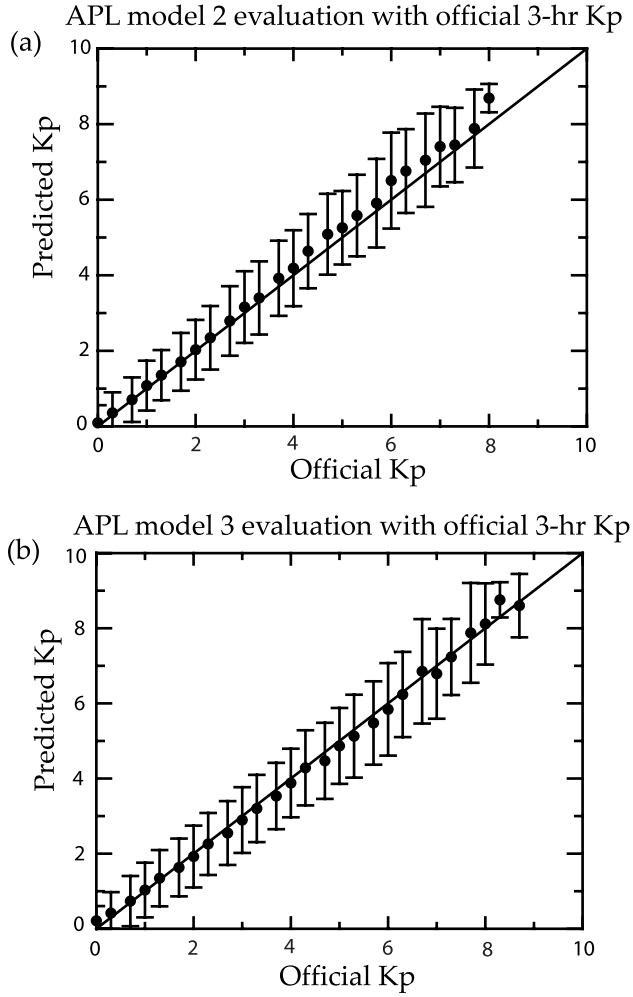

Figure 15. Evaluations with official 3 hour Kp in the same format as Figures 7 and 8 for (a) APL model 2 and (b) APL model 3. The evaluations with official 3 hour Kp and with 15 min interpolated Kp are very similar, as comparisons of the above figures with Figures 7 and 8 reveal.

[46] **Acknowledgments.** We thank NASA CDAWeb for supplying IMP-8, Wind, and ACE Key Parameter data and NOAA for providing ACE data. We also thank MIT for supplying IMP-8 plasma data and GFZ

Postdam for supplying Kp records. S. Wing was supported by NSF Space Weather grant ATM-9819705, NASA grant NAG5-10971 and DOD contract N00024-03-D-6606. J. R. Johnson was supported by NSF grant ATM-0218847 and NASA grant W-19880. We thank J. Vandegriff for assisting with the coding of the recurrent network.

[47] Arthur Richmond thanks Harry C. Koons and another reviewer for their assistance in evaluating this paper.

References

Arge, C. N., and V. J. Pizzo (2000), Improvement in the prediction of solar wind conditions using near-real time solar magnetic field updates, *J. Geophys. Res.*, *105*, 10,465–10,479.

Balikhin, M. A., O. M. Boaghe, S. A. Billings, and H. St C. K. Alleyne (2001), Terrestrial magnetosphere as a nonlinear resonator, *Geophys. Res. Lett.*, *28*, 1123–1126.

Bartels, J. (1949), The standardized index, Ks, and the planetary index, Kp, *IATME Bull.*, *12b*, 97.

Boaghe, O. M., M. A. Balikhin, S. A. Billings, and H. Alleyne (2001), Identification of nonlinear processes in the magnetospheric dynamics and forecasting of Dst index, *J. Geophys. Lett.*, *106*, 30,047–30,066.

Boberg, F., P. Wintoft, and H. Lundstedt (2000), Real time Kp prediction from solar wind data using neural networks, *Phys. Chem. Earth*, *25*, 275–280.

Costello, K. A. (1997), Moving the Rice MSFM into a real-time forecast mode using solar wind driven forecast models, Ph.D. dissertation, Rice Univ., Houston, Texas.

Crooker, N. U., and K. I. Gringauz (1993), On the low correlation between long-term averages of solar wind speed and geomagnetic activity after 1976, *J. Geophys. Res.*, *98*, 59.

Detman, T., and J. A. Joselyn (1999), Real-time Kp predictions from ACE real time solar wind, in *Solar Wind Nine*, edited by S. R. Habbal et al., *AIP Conf. Proc.*, *471*, 729–732.

Fernandez, B., A. G. Parlos, and W. K. Tsai (1990), Nonlinear dynamic system identification using artificial neural networks (ANNs), in *Proceedings of International Joint Conference on Neural Networks 1990*, edited by M. Caudill, pp. 133–141, IEEE Press, Piscataway, N. J.

Fok, M.-C., T. E. Moore, and W. N. Spjeldvik (2001), Rapid enhancement of radiation belt electron fluxes due to substorm dipolarization of the geomagnetic field, *J. Geophys. Res.*, *106*, 3873–3881.

Fry, C. D., W. Sun, C. S. Deehr, M. Dryer, Z. Smith, S.-I. Akasofu, M. Tokumaru, and M. Kojima (2001), Improvements to the HAF solar wind model for space weather predictions, *J. Geophys. Res.*, *106*, 20,985–21,001.

Garrett, H. B., A. J. Dessler, and T. W. Hill (1974), Influence of solar wind variability on geomagnetic activity, *J. Geophys. Res.*, *79*, 4603–4610.

Gehred, P. A., W. Cliffswallow, and J. D. Schroeder III (1995), A comparison of USAF Ap and Kp indices to Gottingen indices, *Tech. Memo. ERL SEL-88*, NOAA, Silver Spring, Md.

Gershenfeld, N. (1999), *The Nature of Mathematical Modeling*, pp. 150–153, Cambridge Univ. Press, New York.

Hakamada, K., and S.-I. Akasofu (1982), Simulation of three-dimensional solar wind disturbances and resulting geomagnetic storms, *Space Sci. Rev.*, *31*, 3–70.

Hardy, D. A., M. S. Gussenhoven, R. Raistrick, and W. J. McNeil (1987), Statistical and functional representations of the pattern of auroral energy flux, number flux, and conductivity, *J. Geophys. Res.*, *92*, 12,275–12,294.

Hedin, A. E. (1987), MSIS-86 thermospheric model, *J. Geophys. Res.*, *92*, 4649.

Johnson, J. R., and S. Wing (2004), A cumulant-based analysis of nonlinear magnetospheric dynamics, *Publ. PPPL-3919*, Princeton Plasma Physics Laboratory, Princeton, N. J. (Available at http://www.pppl.gov/pub_report//2004/PPPL-3919.pdf)

Johnson, J. R., and S. Wing (2005), A solar cycle dependence of nonlinearity in magnetospheric activity, *J. Geophys. Res.*, doi:10.1029/2004JA010638, in press.

Joselyn, J. (1995), Geomagnetic activity forecasting: The state of the art, *Rev. Geophys.*, *33*, 383–401.

Koons, H. C., and D. J. Gorney (1991), A neural network model of the relativistic electron flux at geosynchronous orbit, *J. Geophys. Res.*, *96*, 5549–5556.

Lo, J., and D. Bassu (1999), Mathematical justification of recurrent multilayer perceptrons with long- and short-term memories, in *Proceedings of International Joint Conference on Neural Networks 1999*, vol. 1, pp. 364–369, IEEE Press, Piscataway, N. J.

Mauk, B. H., and C. E. McIlwain (1974), Correlation of Kp with the substorm-injected plasma boundary, *J. Geophys. Res.*, *79*, 3193–3196.

Newell, P. T., S. Wing, C. I. Meng, and V. Sigillito (1990), A neural network based system for monitoring the aurora, *Johns Hopkins APL Tech. Dig.*, *11*(3, 4), 291–299.

Newell, P. T., S. Wing, C. I. Meng, and V. Sigillito (1991), The auroral oval position, structure and intensity of precipitation from 1984 onwards: An automated on-line data base, *J. Geophys. Res.*, *96*, 5877–5882.

Newell, P. T., V. A. Sergeev, G. R. Bikkuzina, and S. Wing (1998), Characterizing the state of the magnetosphere: Testing the ion precipitation maxima latitude (b2i) and the ion isotropy boundary, *J. Geophys. Res.*, *103*, 4739–4745.

Newell, P. T., T. Sotirelis, J. F. Carbary, K. Liou, J. P. Skura, C.-I. Meng, C. Deehr, D. Wilkinson, and F. J. Rich (2002), OVATION: Oval Variation, Assessment, Tracking, Intensity, and Online Nowcasting, *Ann. Geophys.*, *20*, 1039–1047.

Papitashvili, V. O., N. E. Papitashvili, and J. H. King (2000), Solar cycle effects in planetary geomagnetic activity: Analysis of 36-year long OMNI dataset, *Geophys. Res. Lett.*, *27*, 2797–2800.

Rostoker, G. (1972), Geomagnetic indices, *Rev. Geophys.*, *10*, 935–950.

Rumelhart, D. E., and J. L. McClelland (Eds.) (1987), *Parallel Distributed Processing*, vol. I, MIT Press, Cambridge, Mass.

Sergeev, V. A., M. Malkov, and K. Mursula (1993), Testing the isotropic boundary algorithm method to evaluate the magnetic field configuration in the tail, *J. Geophys. Res.*, *98*, 7609–7620.

Takahashi, K., B. A. Toth, and J. V. Olson (2001), An automated procedure for near-real-time Kp estimates, *J. Geophys. Res.*, *106*, 21,017–21,032.

Tsyganenko, N. A. (1989), A magnetospheric magnetic field model with a warped tail current sheet, *Planet. Space Sci.*, *37*, 5–20.

Vandegriff, J., K. Wagstaff, G. Ho, and J. Plauger (2005), Forecasting space weather: Predicting energetic storm particle events using neural networks, *Adv. Space Sci.*, in press.

Wang, Y.-M., and N. R. Sheely (1995), Solar implications of ULYSSES interplanetary field measurements, *Astrophys. J.*, *447*, L143–L146.

Wing, S., and P. Newell (2003), LLBL contribution to the plasma sheet ions, in *Earth's Low-Latitude Boundary Layer*, *Geophys. Monogr. Ser.*, vol. 133, edited by P. T. Newell and T. Onsager, pp. 273–282, AGU, Washington D. C.

Wing, S., P. T. Newell, D. G. Sibeck, and K. B. Baker (1995), Large statistical study of the entry of interplanetary magnetic field Y-component into the magnetosphere, *Geophys. Res. Lett.*, *22*, 2083–2086.

Wing, S., R. A. Greenwald, C.-I. Meng, V. G. Sigillito, and L. V. Hutton (2003), Neural Networks for automated classification of ionospheric irregularities from HF radar backscattered signals, *Radio Sci.*, *38*(4), 1063, doi:10.1029/2003RS002869.

Wu, J., and H. Lundstedt (1997), Geomagnetic storm predictions from solar wind data with the use of dynamic neural networks, *J. Geophys. Res.*, *102*, 14,255–14,268.

M. Balikhin, Department of Automatic Control and System Engineering, University of Sheffield, Mappin Street, Sheffield S1 3JD, UK.

K. Bechtold, J. Jen, C.-I. Meng, K. Takahashi, and S. Wing, Johns Hopkins University Applied Physics Laboratory, 11100 Johns Hopkins Road, Laurel, MD 20723-6099, USA. (simon.wing@jhuapl.edu)

K. Costello, NASA Lyndon B. Johnson Space Flight Center, 2101 NASA Parkway, Houston, TX 77058, USA.

J. Freeman, Physics and Astronomy Department, Rice University, P. O. Box 1892, Houston, TX 77005, USA.

J. R. Johnson, Princeton Plasma Physics Laboratory, Princeton University, P. O. Box 451, MS 28, Princeton, NJ 08543-0000, USA.

D. G. Sibeck, NASA Goddard Space Flight Center, LEP Code 696, 8800 Greenbelt Road, Greenbelt, MD 20771, USA.